Alkali Metal Borate Conjugated Block Polyelectrolytes as Tuneable Mixed Ionic-Electronic Conductors

Sebastian J. Leeming,[a] Samuel Fryer,[a] Georgina L. Gregory* [a]

[a] Chemistry Research Lab, University of Oxford, 12 Mansfield Road, Oxford, OX1 3TA

Email: georgina.gregory@chem.ox.ac.uk

Table of Contents

Materials and Reagents

All reagents and anhydrous solvents were purchased from Sigma Aldrich and used as received unless otherwise noted. ***Monomers:*** M1 was synthesised following the procedure described by Carillo *et al.*[1], which starts from 2-bromo-3-hexylthiophene purchased from Tokyo Chemical Industries (TCI) and bis(trimethylsilyl) *N*-methylimidoacetic ester (**TMS_2-MIDA)** synthesised as a yellow oil (13.75 g, 43% yield) following the literature procedure.[2] Allyloxymethyl-2-Ethyltrimethylene Carbonate **(AEC)** was synthesised as a colourless liquid (13.8 g, 58% yield) following procedures described elsewhere (e.g. by Brandell and coworkers[3]) from trimethylolpropane allyl ether (Sigma) using 1,1'-carbonyldiimidazole (CDI reagent, TCI). Methoxypolyethylene glycol epoxide (mPEO-EPO), purchased from Creative PEGWorks or Biopharma PEG (44-45 EO units PEG) was dried by dissolving in anhydrous THF and stirring over calcium hydride (CaH_2) for at least 24 hours prior to cannula filtration and drying *in vacuo*. All monomers were then stored in an argon-filled glovebox freezer at -30 °C. ***Polymers:*** All synthesised conjugated polyelectrolytes were dried under vacuum and stored in an Argon-filled glovebox.

Characterisation Techniques

Nuclear Magnetic Resonance Spectroscopy (NMR): ^{1}H, ^{7}Li, $^{11}B\{^{1}H\}$, $^{13}C\{^{1}H\}$, ^{23}Na, $^{31}P\{^{1}H\}$ NMR spectra were recorded with a Bruker Avance III HD nanobay NMR equipped with a 9.4 T magnet. ^{39}K NMR spectra were recorded with a Bruker Avance III HD NMR equipped with an 11.75 T magnet. To overcome challenges in analysis arising from a steep baseline in the ^{39}K spectra, an exponential window multiplication was applied to determine how many excess data points needed to be removed. Once removed, the analysis was conducted as normal.

Size Exclusion Chromatography (SEC): Prior to derivatisation as a metal borate, the polymers (5-10 mg) were dissolved in THF before being passed through a 0.2 µm PTFE filter. Analysis of P3HT homopolymers was performed on a Shimadzu LC020AD instrument with a Refractive Index (RI) and UV detector with two PSS SDV 5 µm linear M columns. Narrow monodisperse polystyrene standards were used for calibration. For block copolymers an Agilent LC1260 Infinity II System was used fitted with PLgel 5 µm MIXED-C analytical columns, and a refractive Index detector (RI) detector. Easy-M narrow polystyrene standards were used for calibration. GPC grade THF (BHT stabilised) was used as the eluent at a flow rate of 1.0 mL min^{-1} and a column temperature of 35 °C.

Phosphorus End Group Test: Following previous reports, for example by the Williams Group,[4] -OH terminated polymers (20 mg) were dissolved in chloroform ($CDCl_3$; 0.4 mL). A solution (~20 µL) of $Cr(acac)_3$ (5.5 mg) and internal standard Bisphenol A (BPA; 400 mg) in pyridine (10 mL) were added. Then, 2-chloro-4,4,5,5-tetramethyl dioxaphospholane (20 µL per end group present) was added and the sample analysed by $^{31}P\{^1H\}$ NMR spectroscopy.

MALDI-ToF Mass Spectrometry: Polymer samples (5 mg) dissolved in THF (1 mL) were mixed with a solution of sodium or potassium trifluoroacetate (0.1 M in THF). To this solution was then added a freshly prepared solution of matrix, trans-2-[3-(4-tert-Butylphenyl)-2-methyl-2-propenylidene]malononitrile (DCTB) (10 mg per mL THF). The matrix, polymer and salt solutions were combined in a 1:1:1 ratio by volume. The solution mixture was then spotted (2-5 µL) onto a Bruker stainless steel MALDI plate and the solvent left to evaporate in air. A Bruker Autoflex Speed MALDI-TOF instrument was then used in reflector positive (RP) mode with 5-20 kDa range. A matrix suppression of 1000 Da was employed with PEG calibration 33kDa. The spectra were cumulatively added to obtain an intensity of > 10^4. Flex analysis software was used to analysis the data.

Differential Scanning Calorimetry (DSC): DSC measurements were recorded on a TA instruments DSC25 instrument calibrated with sapphire and Indium standards. Measurements were recorded at a heating and cooling rate of 10 °C min^{-1} in hermetically sealed Al pans. Samples were cooled to and equilibrated at -80 °C before being heated to 100 °C and then cooled back -80 °C, under a flow of N_2 (80 mL min^{-1}). This was repeated twice to remove any thermal history from the sample. Glass transition temperatures (T_g) were measured from the midpoint of the transition in the third heating curve. Melt temperatures (T_m) were measured from the minimum in the peak of the third heating curve.

Thermogravimetric Analysis (TGA): TGA was measured on a TGA5500 machine (TA instruments). Samples were heated at a rate of 10 °C min^{-1} from 40 °C to 500 °C under a flow of N_2 (100 cm^3 min^{-1}).

Electrochemical Impedance (EIS) and Dielectric Relaxation Spectroscopy (DRS): Vacuum-dried CBEs were hot-pressed into PTFE O-ring spacers (0.9 mm thick, 8 mm internal diameter) using a Carver hot-press (4386CE) at 40–70 °C, sufficiently below the degradation onset for each material. The PTFE spacers maintained consistent sample thickness during heating cycles. Films were visually inspected under a digital microscope (1200× magnification) to confirm they were bubble-free. Sample thickness was recorded before and after

measurement using callipers (three points per sample) and verified with a BioLogic thickness measurement kit. The polymer films were loaded into a BioLogic cell holder between two gold blocking electrodes (6.35 mm diameter) within an argon-filled glovebox to minimise moisture uptake. This assembly was inserted into a BioLogic Controlled Environment Sample Holder (CESH-e) for air-free, temperature-controlled measurements, with a 100 N spring load applied to maintain electrode contact. Impedance measurements were conducted using a BioLogic MTZ-35 impedance analyser over a frequency range of 35 MHz to 100 kHz at 10 mV AC amplitude with no DC bias. Spectra were recorded at 10 °C intervals from 70 to 30 °C, with a 30 min thermal equilibration at each temperature. Temperature was controlled using a BioLogic ITS-e temperature chamber. Three repeat measurements were conducted on two separate samples of each polymer. Using EC-Lab software, impedance data (Z', Z'') were fit to an equivalent circuit: $CPE_1/(R_1 + CPE_2/R_2)$, where CPE denotes a constant phase element. Bulk resistance ($R_{bulk} = R_2$), corresponding to the x-intercept of the semicircle in Nyquist plots, was extracted from these fits. Ionic conductivity (σ_i) was calculated as:

$$\sigma_i = \frac{t}{R_{bulk} \times A}$$

Where A is the electrode area (31.67 mm^2), and t is the polymer film thickness (ca. 0.9 mm

For DRS measurements, the same experimental configuration was employed, with raw data converted to complex permittivity (ε', ε'') to analyse dipolar relaxations, segmental dynamics, and ion hopping processes.

Linear Sweep Voltammetry (LSV): These were measured using the same cell set-up as above for EIS but conducted using a BioLogic SP-150e Potentiostat. Current-voltage curves were conducted from the open circuit voltage (OCV) to the OCV + 2 V at a scan rate of 1 mV s^{-1}. Samples were stabilised at the OCV for at least 1 hour before LSV measurements. Samples were heated using a BioLogic ITS-e temperature chamber.

Chronoamperometry (CA): Samples were prepared and loaded into the same cell set-up as for EIS and LSV above. These measurements were conducted using a BioLogic SP-150e Potentiostat by applying a voltage bias of 1.5 V versus the OCV for 1-2 hours during which time the current (I) was recorded as a function of time until the steady state current (I_{SS}) was reached (plateau). These were conducted at temperatures controlled by the ITS-e temperature control system after a 30 min soak time. Electronic conductivity (σ_e) could be calculated:

$$\sigma_e = \frac{I_{SS} \times L}{V \times A}$$

Where V = applied voltage, L =sample thickness and A = electrode area (=πr^2=31.67 mm^2).

Rheology: Polymer discs were prepared by hot-pressing as described above for electrochemical measurements. The polymers discs were then placed between two 8 mm stainless steel plates on an ARES-G2 (TA instruments) rheometer. Shear storage (*G*') and loss (*G*'') moduli were recorded. Amplitude sweeps (0.01 to 10%) were used to determine the amplitude strain at which the polymers remained in the linear viscoelastic region (LVR) – typically 0.1 or 1% strain. These amplitude strains were used to conduct frequency sweeps from 100 Hz to 0.1 Hz at 60 °C. The data was analysed using TRIOS software.

Tensile Testing. Dumbbell-shaped specimens were cut using a ZwickRoell or Ray-Ran Hand Operated cutting press equipped with a dog bone sample cutter for ISO 527-2 type 5B. Uniaxial tension experiments were conducted at different cross-head speeds on a Instron 3340 universal tester with a 50 N capacity, force calibrated to standard ISO 7500-1.

Monomer Synthesis

5-bromo-4-n-hexylthien-2-yl-MIDA-boronate (M1):[1] Under an inert atmosphere, $AlCl_3$ (2.70 g, 20.3 mmol, 1.01 equiv.) and 2,6-dichloropyridine (3.56 g, 24.1 mmol, 1.20 equiv.) were dissolved in anhydrous dichloromethane (DCM, 60 mL). Then boron trichloride (BCl_3, 20.25 mL, 20.3 mmol, 1.01 equiv.) was added and the reaction mixture cooled to 0 °C before adding 2-bromo-3-hexylthiophene (4.96 g, 20.1 mmol, 1.00 equiv.). After stirring the reaction at ambient temperature for 1 h, *N,N*-dimethyl-*p*-toluidine (2.74 g, 20.3 mmol, 1.01 equiv.) was added and the solution immediately transferred *via* cannula to a solution of TMS_2-MIDA (6.13 g, 21.1 mmol, 1.05 equiv.) in acetonitrile (50 mL). After 14 h, the volatiles were removed *in vacuo* and the crude product extracted in DCM before being washed with water (3 x 100 mL), brine (1 x 100 mL), and the organic phase dried over $MgSO_4$. The product was further purified by flash column chromatography (Biotage®, 40 g silica column) eluting with a gradient of DCM/hexane 0:1 →DCM/hexane 1:1 → ethyl acetate (EA)/ DCM 1:9 → DCM 1:1. The combined EA/DCM fractions were concentrated under reduced pressure and dried to yield a pale yellow crystalline solid (2.4632 g, 30.5%). **^{1}H ($CDCl_3$)/ppm**: 7.00 (1H, s, thiophene-ring C-H), 4.24 (2H, d, MIDA-CH2), 3.87 (2H, d, MIDA-CH2), 2.68 (3H, s, MIDA-N-**CH_3**), 2.49 (2H, *t*, thiophene-**CH_2**-C_5H_{11}), 1.52 (2H, *dd*, hiophene-CH_2-**CH_2**-C_4H_9) (6H, s, thiophene-C_2H_4-**CH_2-CH_2-CH_2**-CH_3), 0.85 (3H, t, thiophene-C_5H_{10}-**CH_3**). **^{13}C{^{1}H} ($CDCl_3$)/ppm**: 168.72 (C=O, MIDA),

144.12 (thiophene, quaternary, C-3), 134.84 (thiophene, CH, C-4), 113.32 (thiophene, quaternary, C(2)-Br), 61.74 (MIDA, CH2), 47.93 (MIDA, CH3), 31.59, 29.78, 29.47, 29.03 (Hex), 22.65 (Hex), 14.15 (Hex-CH3). %). **HR-MS (ESI)**: calcd. for $C_{15}H_{20}BBrNO_4S^-$ $[M - H^+]^-$ 400.0394 m/z, found 400.0404 m/z.

2-allyloxymethyl-2-ethyltrimethylene carbonate (AEC):[3] Under an inert atmosphere, trimethylolpropane allyl ether (TMPAE; 20.9 g, 120 mmol, 1 equiv.) was dissolved in dry dichloromethane (DCM; 320 mL, 0.375 M) and 1,1'-carbonyldiimidazole (CDI; 24.3 g, 150 mmol, 1.25 equiv.) was gradually added to the solution in twelve batches over the course of 1 h. After which, the solution was immediately washed with 1M hydrochloric acid (2x 320 mL) and the organic phase dried over Mg_2SO_4, before removing the DCM *in vacuo* to afford AEC as a colourless liquid (13.8 g, 58 % yield). ^{1}H ($CDCl_3$)/ppm: 5.82 (1H, m, **H**C=CH_2), 5.17-5.42 (2H, m, HC=C**H$_2$**), 4.28 (2H, *d*, ring-CH_2), 4.12 (2H, *d*, ring-CH_2), 3.94 (2H, *d*, -O**CH$_2$**-CH=CH_2), 3.36 (2H, s, -**CH$_2$**-O-CH_2-), 1.48 (2H, *q*, -**CH$_2$**-CH_3), 0.87 (3H, s, -CH_2-**CH$_3$**).

P3HT-OH Macroinitiators

P3HT-OH macroinitiators were synthesised from M1 via SCTP.[5] To a round bottom flask charged with magnetic stirrer, 4-iodobenzylalcohol (4.7 mg, 0.02 mmol, 1 equiv.), RuPhos-Pd-G3 catalyst (G3 cat.; 17 mg, 0.02 mmol, 1.1 equiv.), RuPhos ligand (14 mg, 0.03 mmol, 1.5 equiv.), and K_3PO_4 (1.27 g, 0.12 mmol, 6 equiv.) were added before adding THF (10 mL) and water (3.6 mL, 0.2 mmol, 5 equiv.). The solution was heated to 50 °C for 1 h to activate the initiator before cooling to 45 °C and adding via cannula transfer a solution of M1 (402 mg, 0.01 mmol, 50 equiv.) in THF (85 mL). The reaction mixture was then left to stir at this temperature for 14-48 h, during which a colour change from yellow to bright orange to dark red was observed. The polymerisation was then quenched with HCl (6M, 25 mL), diluted with chloroform and the organic phase washed with brine (3×200 mL), concentrated and finally precipitated into cold methanol before being isolated by vacuum filtration as a violet to gold powder/film (depending on DP) and dried in vacuo ($P3HT_{35}$-OH: 154 mg, 80 %).

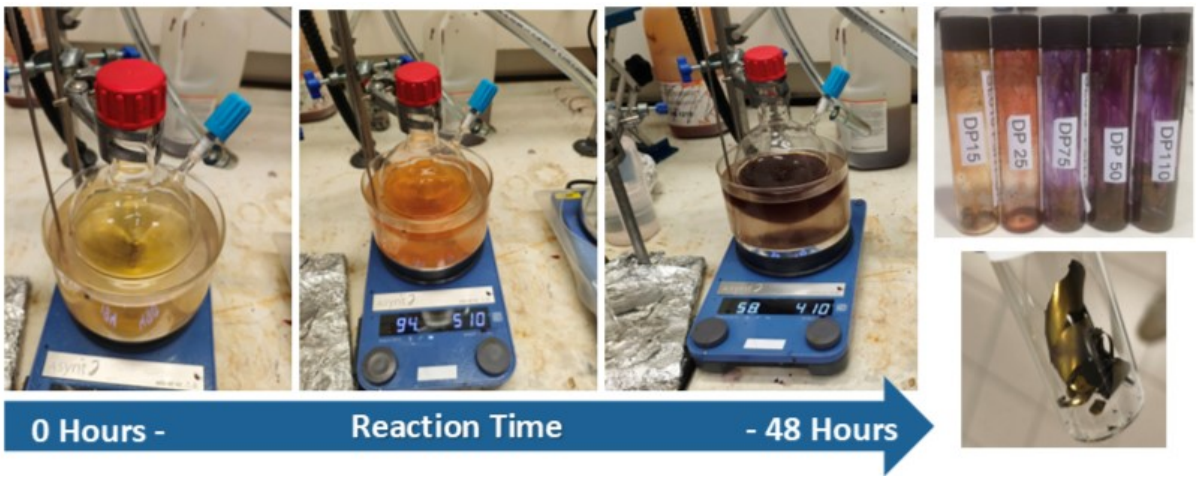

Table S1. Summary of P3HT-OH synthesised via SCTP (Fig. 1A).

[I] mmol	[M]/[I]	P3HT-OH product					
		$M_{n,\ theory}$ (g mol^{-1})[a]	$M_{n,\ NMR}$ (g mol^{-1})[b]	DP_{NMR}	$M_{n,\ SEC}$ (g mol^{-1})[c]	$Đ$	rr (%)[d]
0.067	15	2600	2265	13	3030	1.18	88
0.067	15	2600	4091	24	4090	1.33	86
0.0285	35	5947	5585	33	6960	1.29	90
0.02	50	8422	9403	56	8670	1.41	87
0.0133	75	12572	11561	69	10300	1.75	90
0.008	125	20872	18035	108	18200	1.37	92

[a] $M_{n,\ theory}$ determined by the ratio of M1 to iodobenzyl alcohol initiator put into the reaction (i.e., DP_{theory} × 402.11). [b] $M_{n,\ NMR}$ was calculated from the integration ratio of benzyl alcohol aromatic protons (7.5 ppm) to the P3HT thiophene proton (6.9 ppm). If significant populations of polymer chains lacked the benzyl alcohol end-group, this would result in overestimation of $M_{n,NMR}$ due to reduced initiator signal intensity. [c] $M_{n,\ SEC}$ from refractive index (RI) measurements. [d] ***rr* (%)** was calculated from the integration percentage of the different thiophene alkyl proton environments (2.81 ppm/ (2.81 + 2.60 ppm).

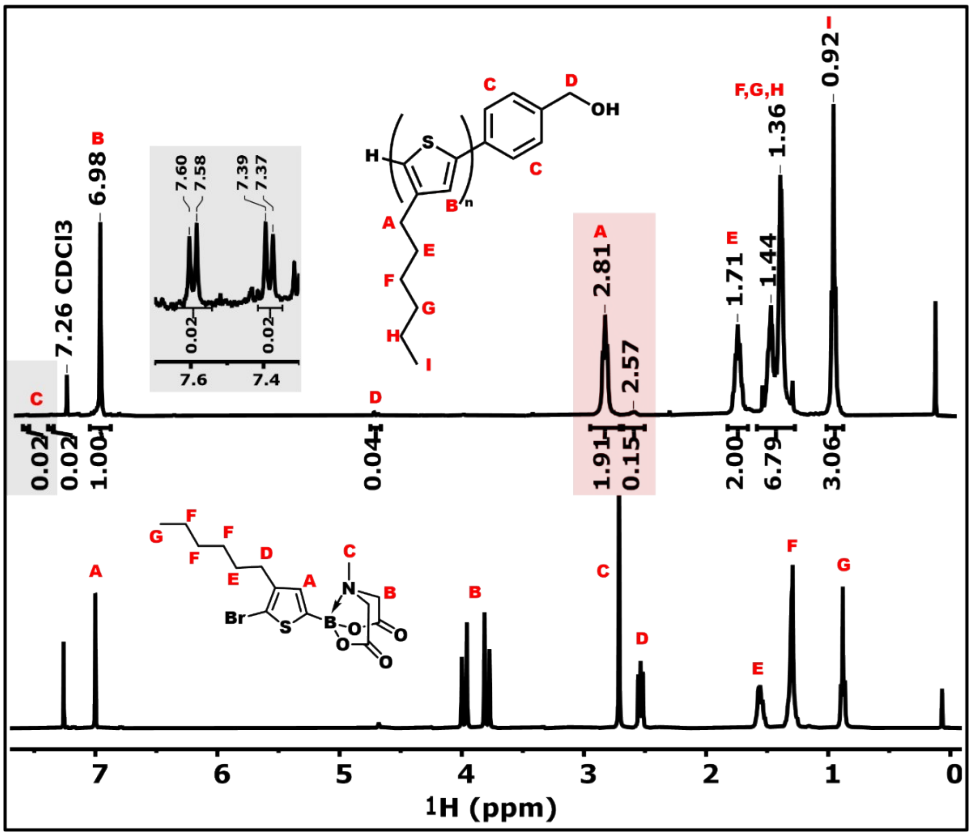

Fig. S1: ^{1}H NMR stack (400 MHz, $CDCl_3$) of M1 and P3HT-OH.

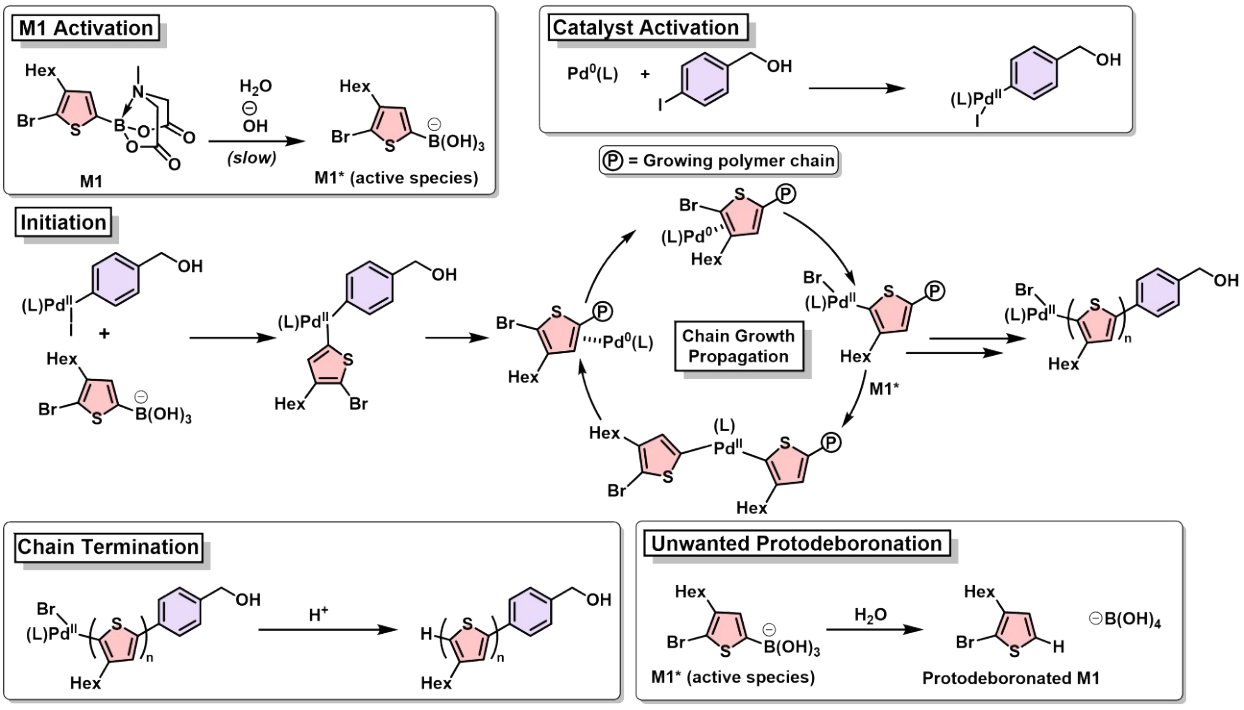

Scheme S1: SCTP mechanism as proposed by [2, 6]

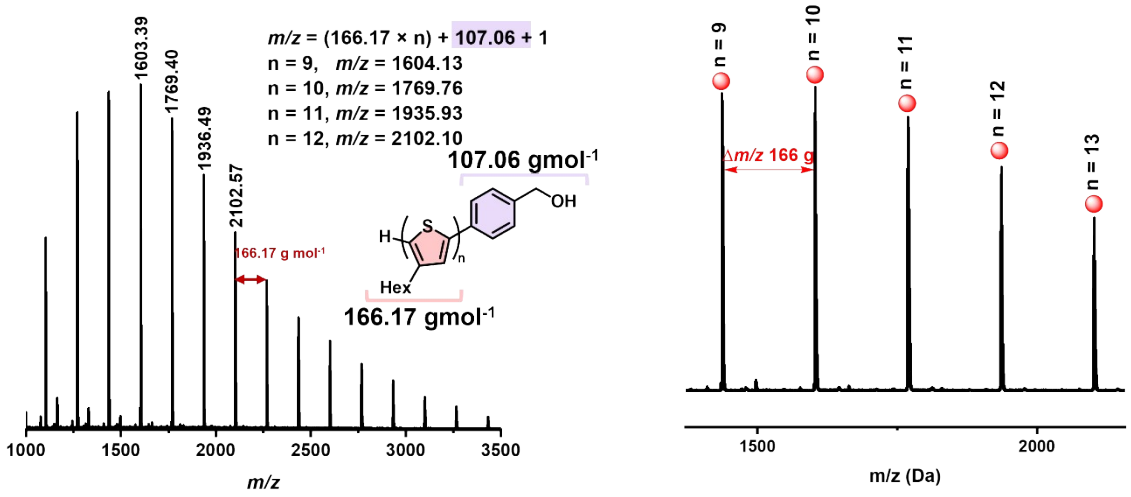

Fig. S2: MALDI-ToF mass spectrometry (DCTB matrix) of P3HT$_{15}$-OH.

Synthesis of ABC-type Triblock Copolymers

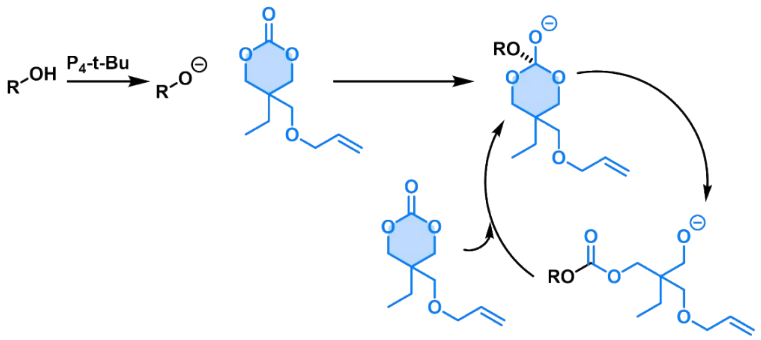

Scheme S2: Phosphazene organobase-catalysed ROP mechanism.

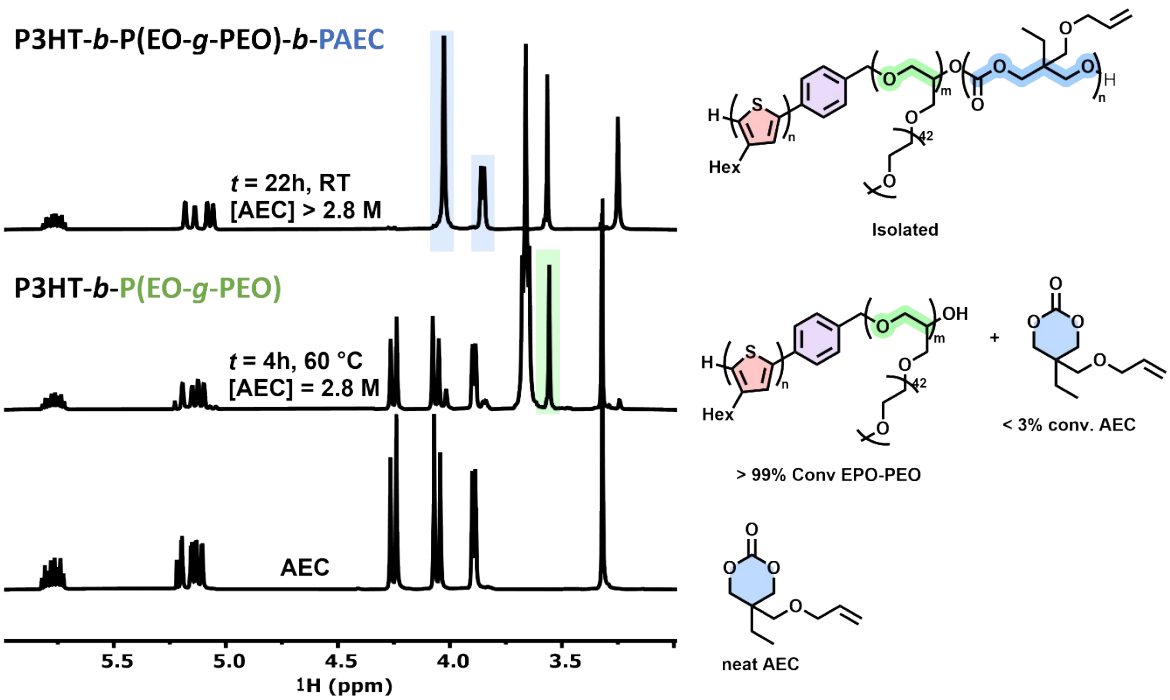

Fig. S3: ^{1}H NMR (400 MHz, $CDCl_3$) of sequential EPO-PEO and AEC ROP (Fig. 1B).

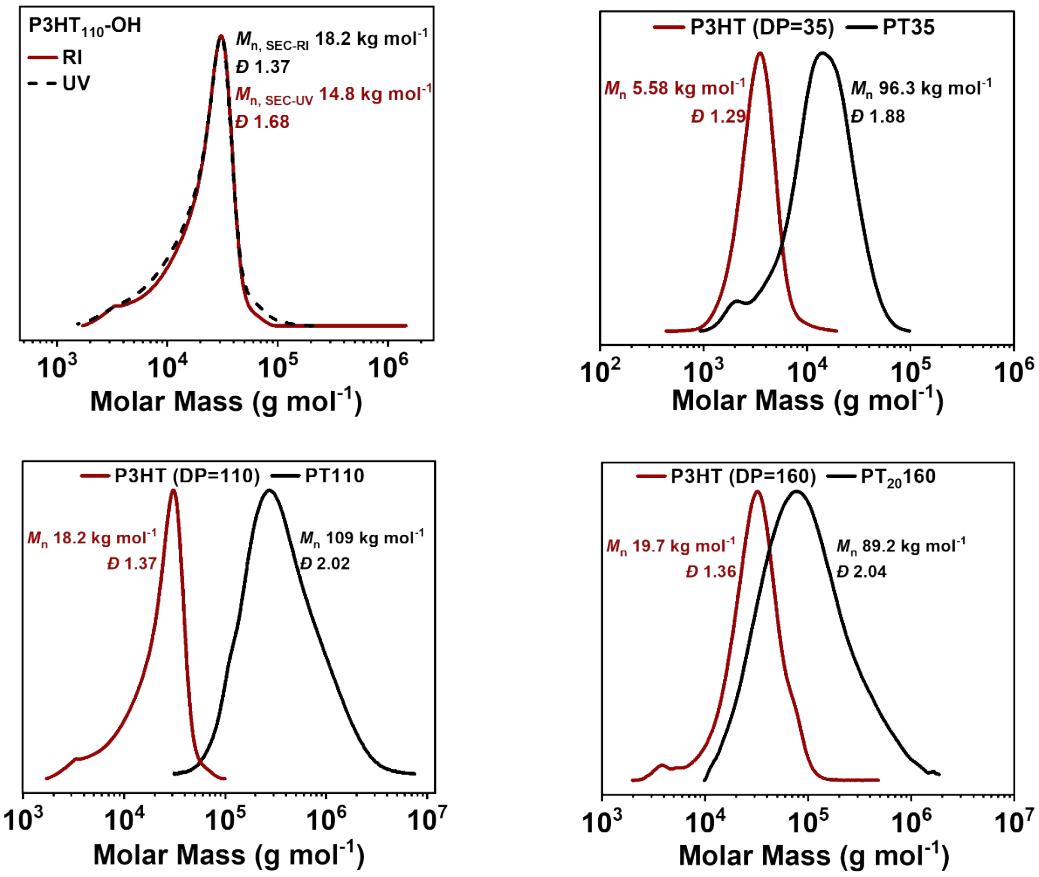

Fig. S4. SEC traces (THF eluent, RI detector) for P3HT-OH and P3HT-*b*-P(EO-*g*-PEO)-*b*-PAEC.

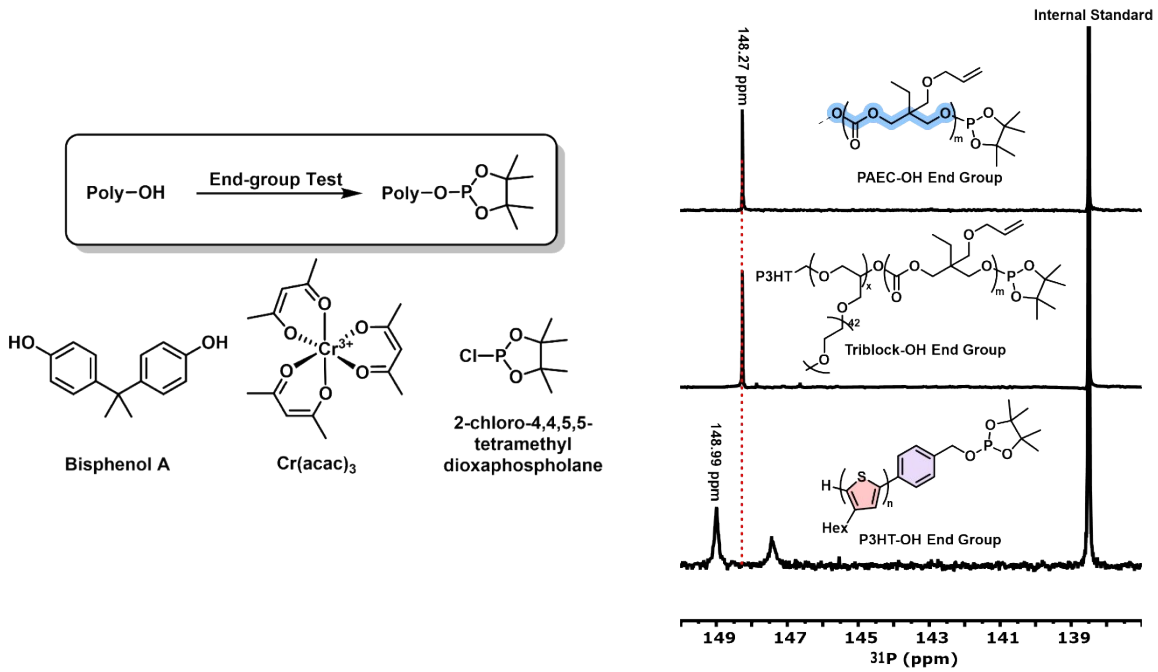

Fig. S5: End-group test $^{31}P\{^{1}H\}$ NMR spectra (400 MHz, $CDCl_3$).

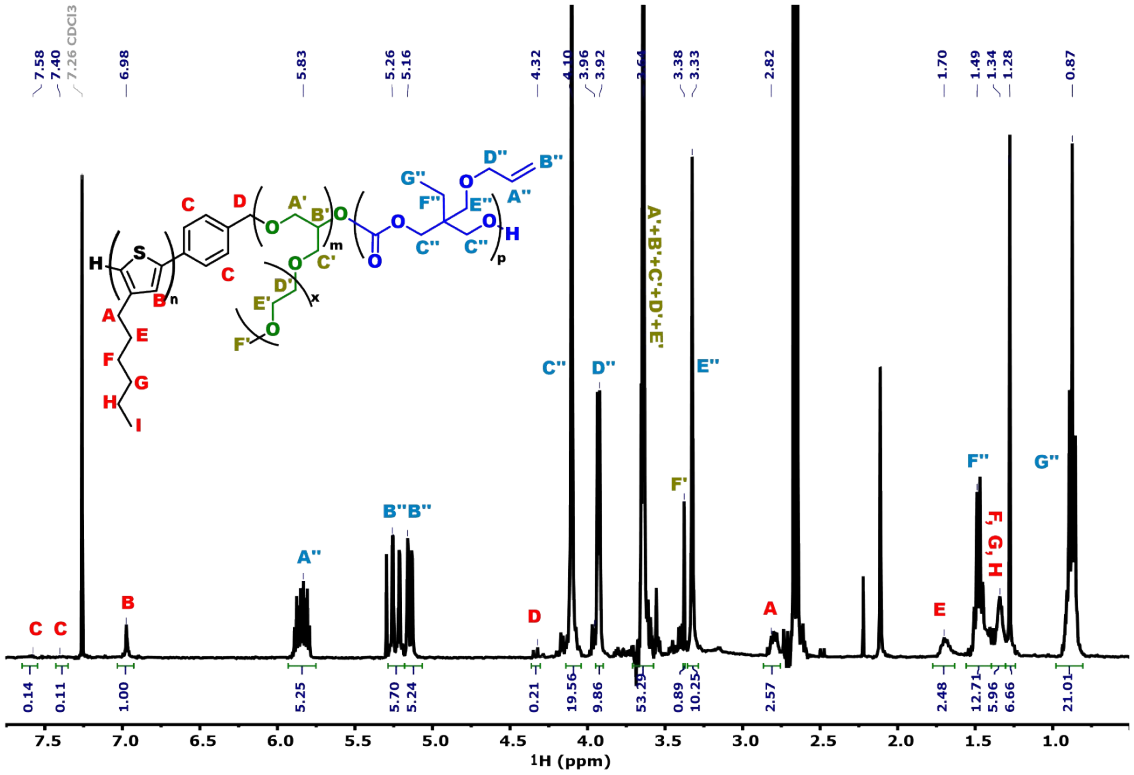

Fig. S6: ^{1}H NMR spectra ($CDCl_3$, 400 MHz) of P3HT$_{33}$-*b*-P(EO-*g*-PEO)$_2$-*b*-PAEC$_{269}$ (Table 1, Entry 2).

Alkali Metal Borate CBEs

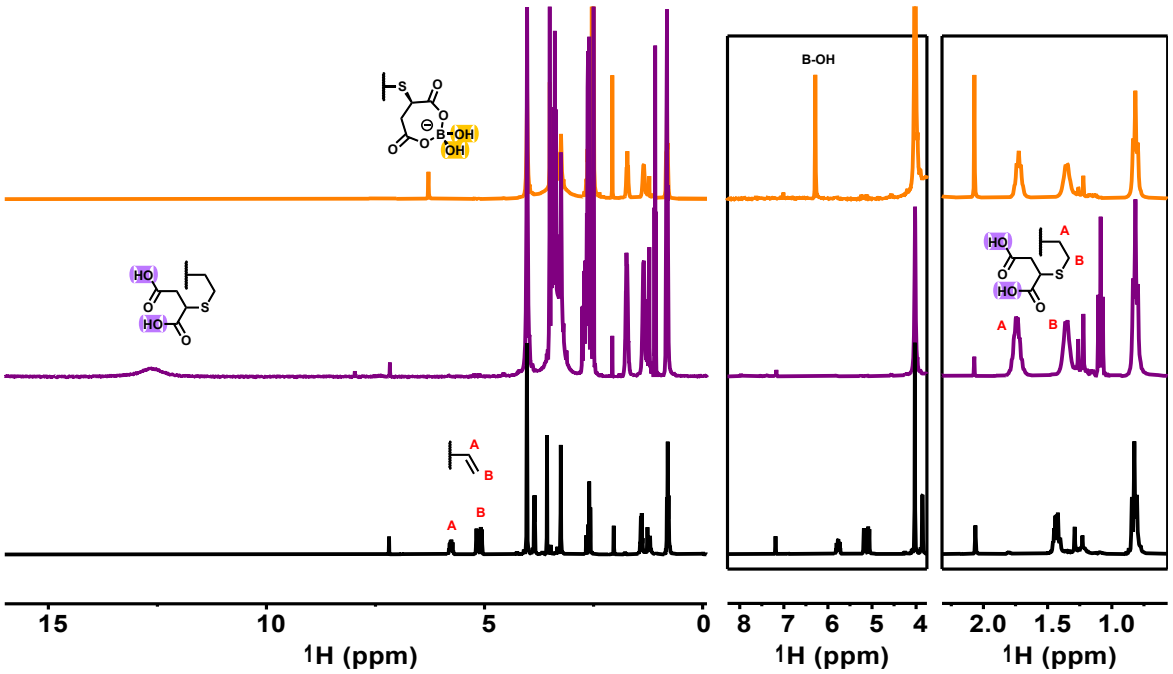

Fig. S7: ^{1}H NMR (400 MHz, DMSO-d_6) stack showing conversion of vinyl to diacid to borate.

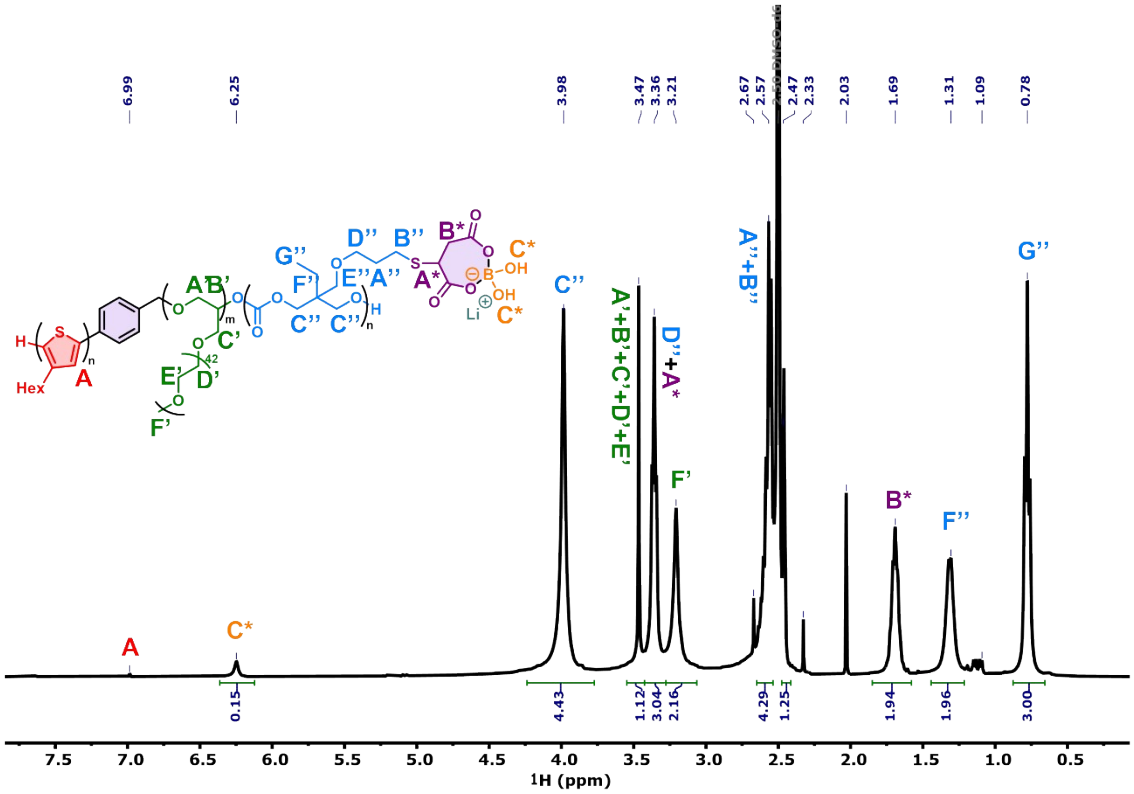

Fig. S8: Representative ^{1}H NMR (400 MHz, DMSO-d_6) spectra of CBE-$BO_4^-M^+$.

Differential Scanning Calorimetry (DSC)

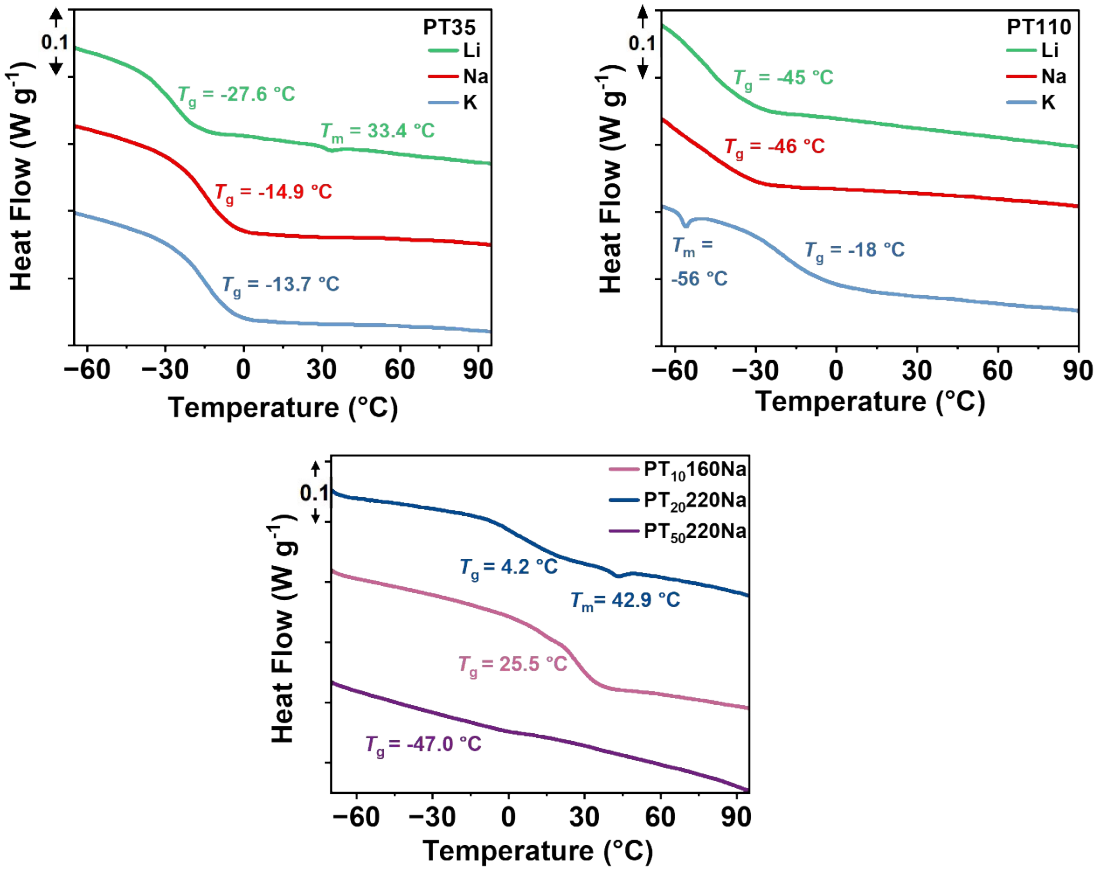

Fig. S9: DSC thermograms (3rd heating cycle) (Fig. 2).

Thermogravimetric Analysis (TGA)

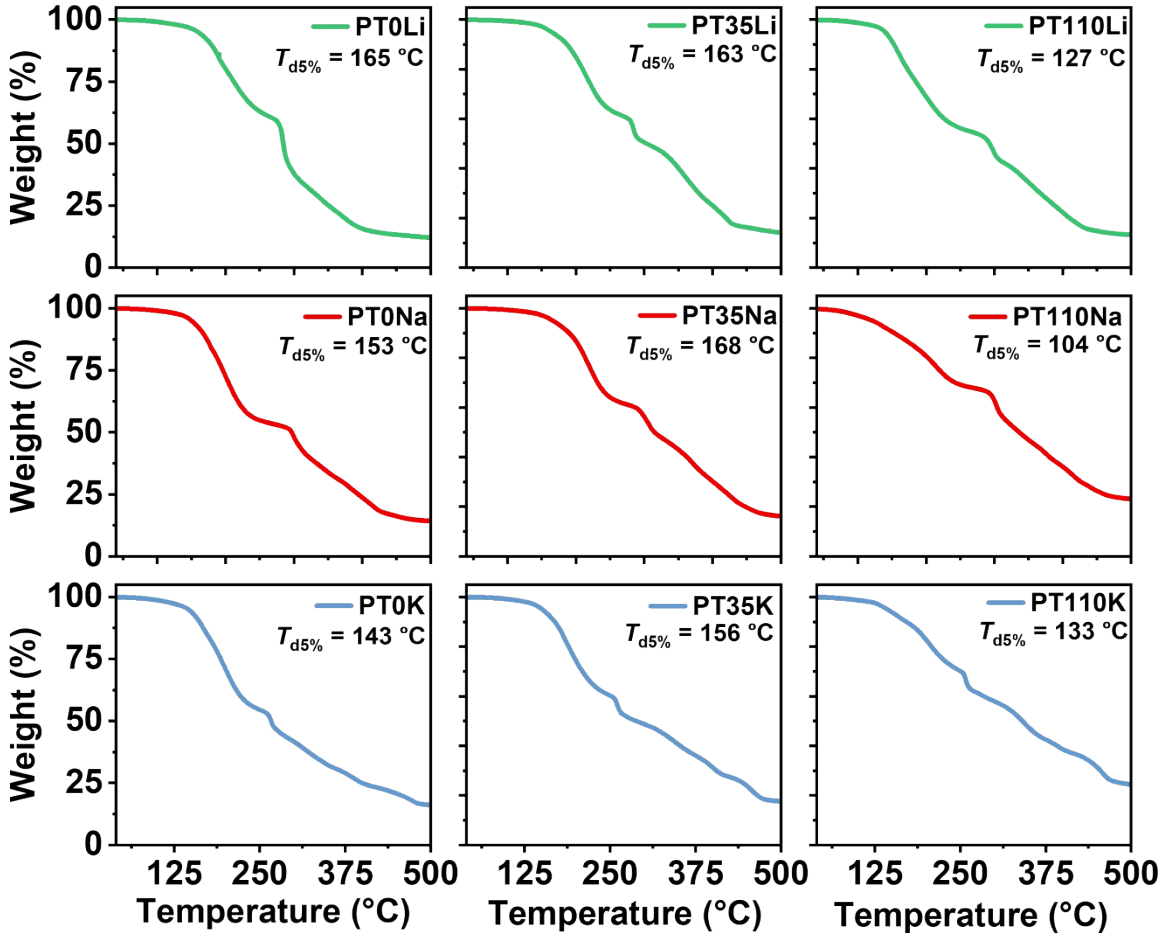

Fig. S10: TGA curves for CBEs.

Additional Rheology Data

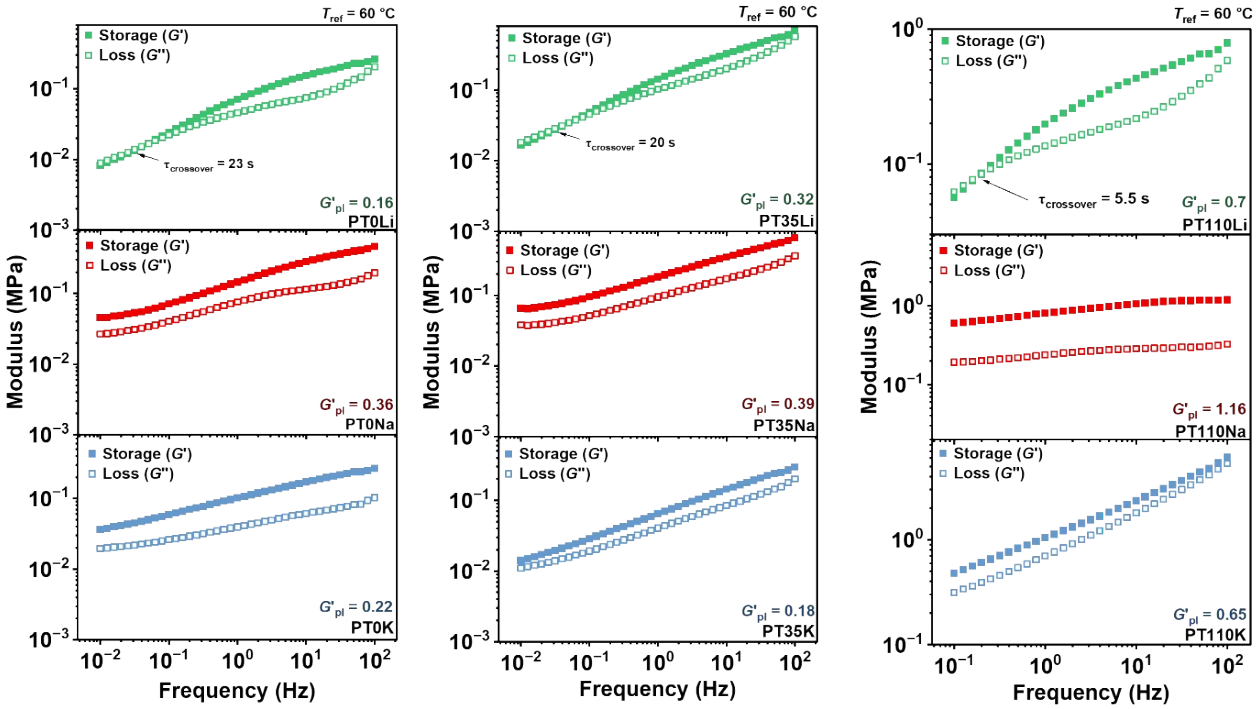

Fig. S11: Frequency sweeps at 60 °C.

Ionic Conductivity

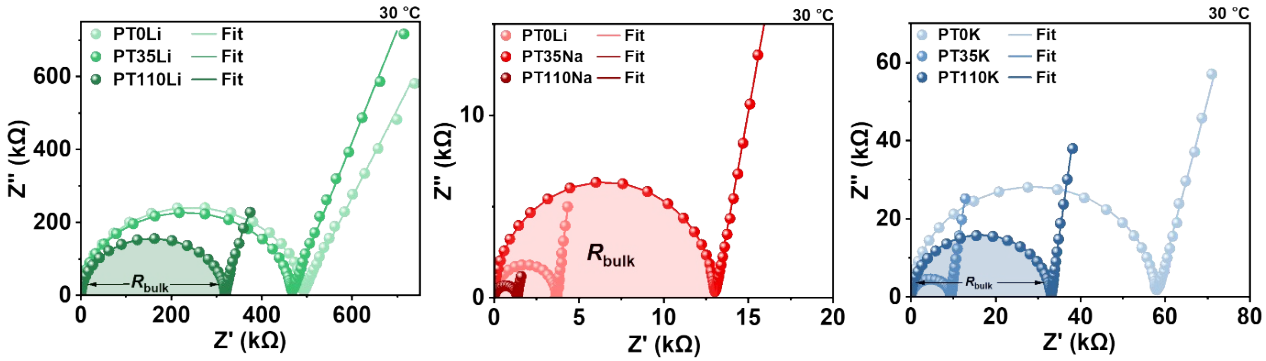

Fig. S12: Nyquist Curves with equivalent circuit fits (Fig. 3).

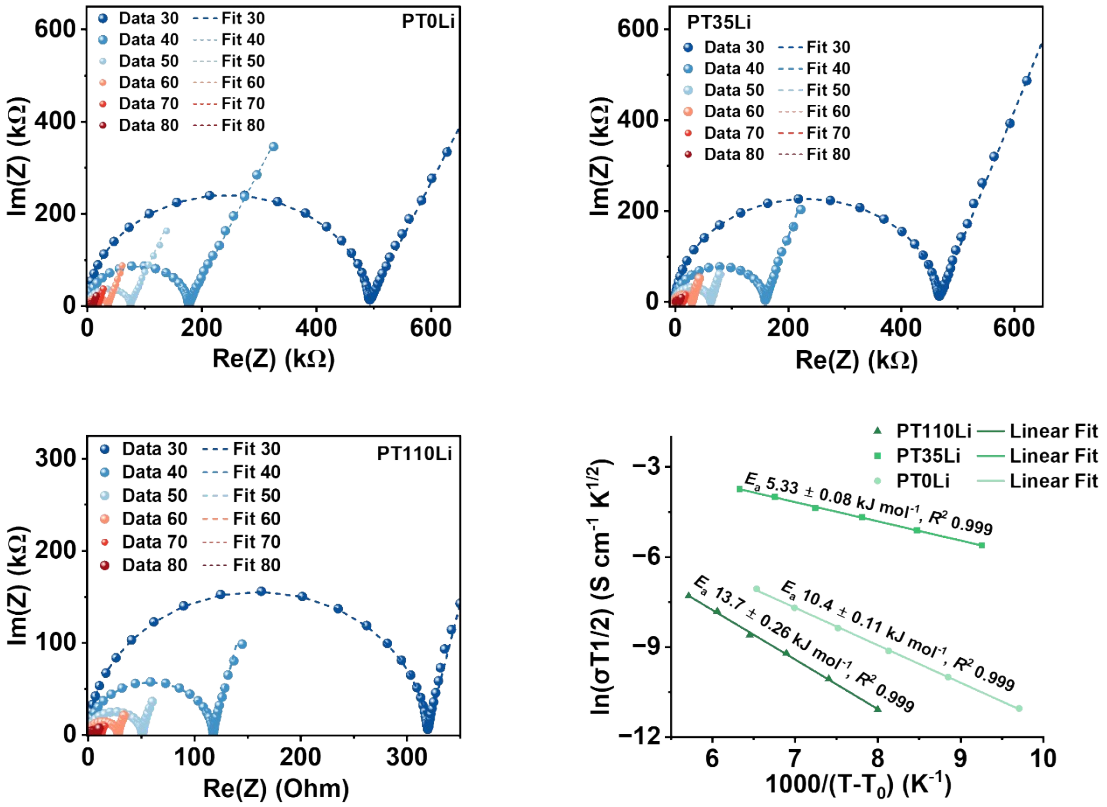

Fig. S13: VTF fits for Li^+ (Fig. 3B & C).

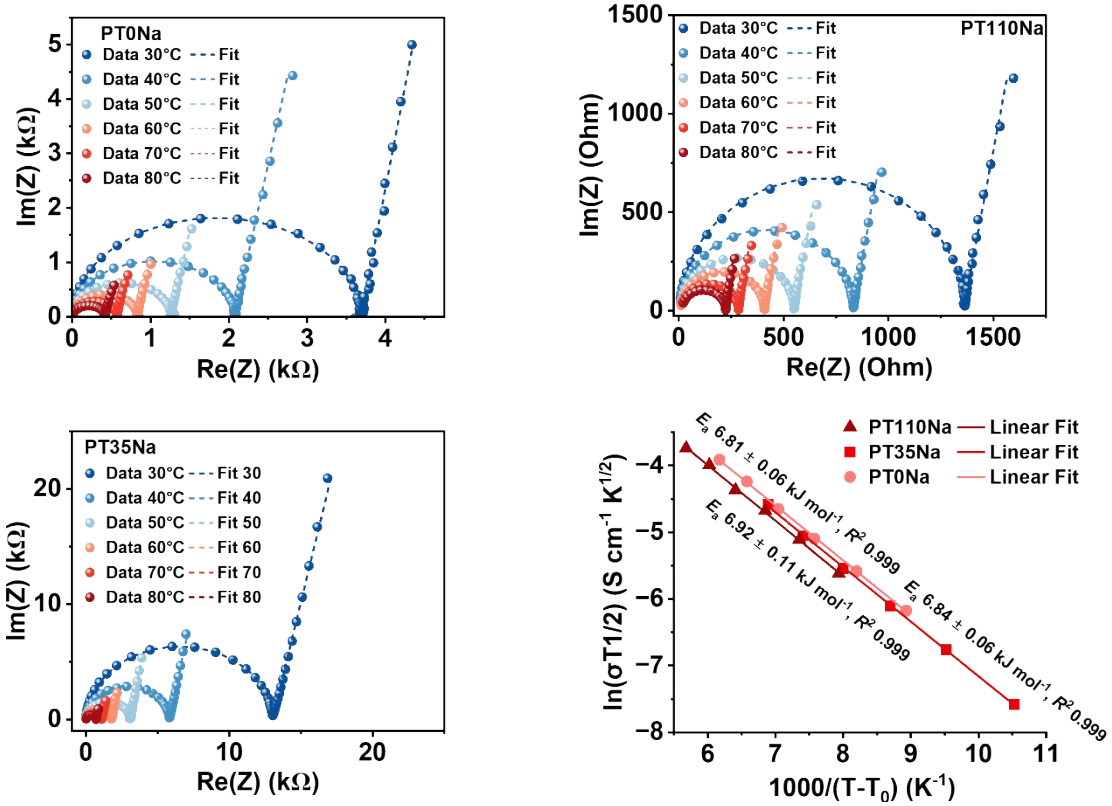

Fig. S14: VTF fits for Na^+ (Fig 3B & C).

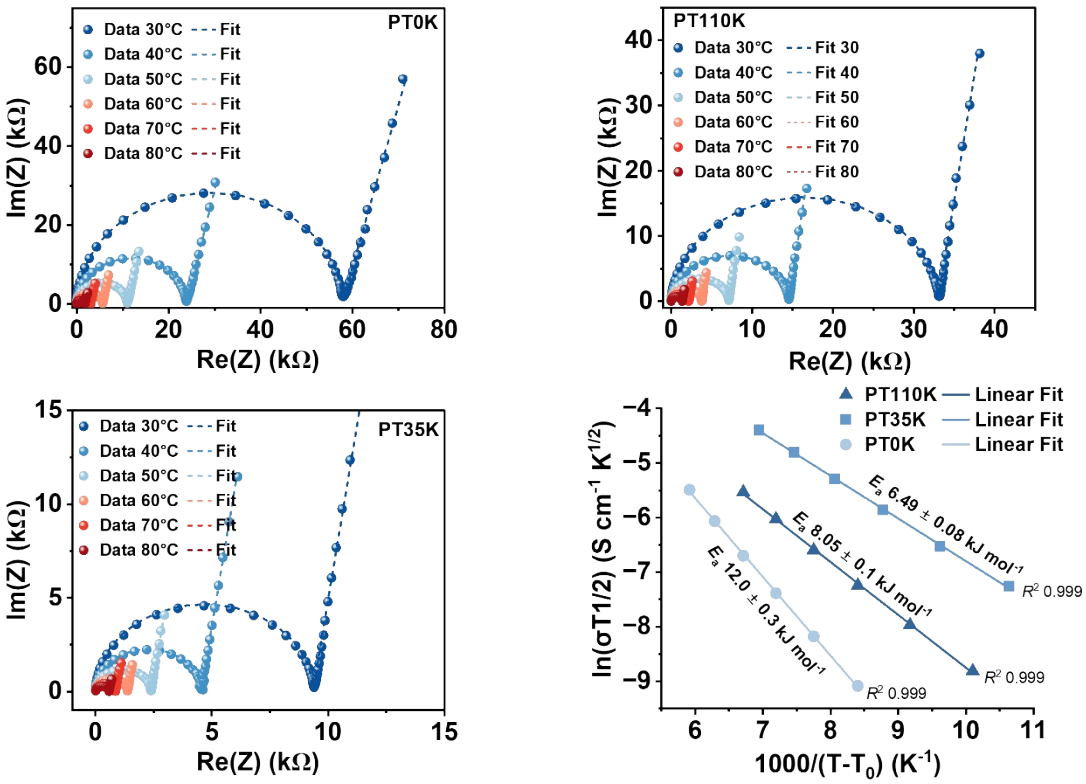

Fig. S15: VTF fits for K^+ (Fig 3B & C).

Electronic Conductivity

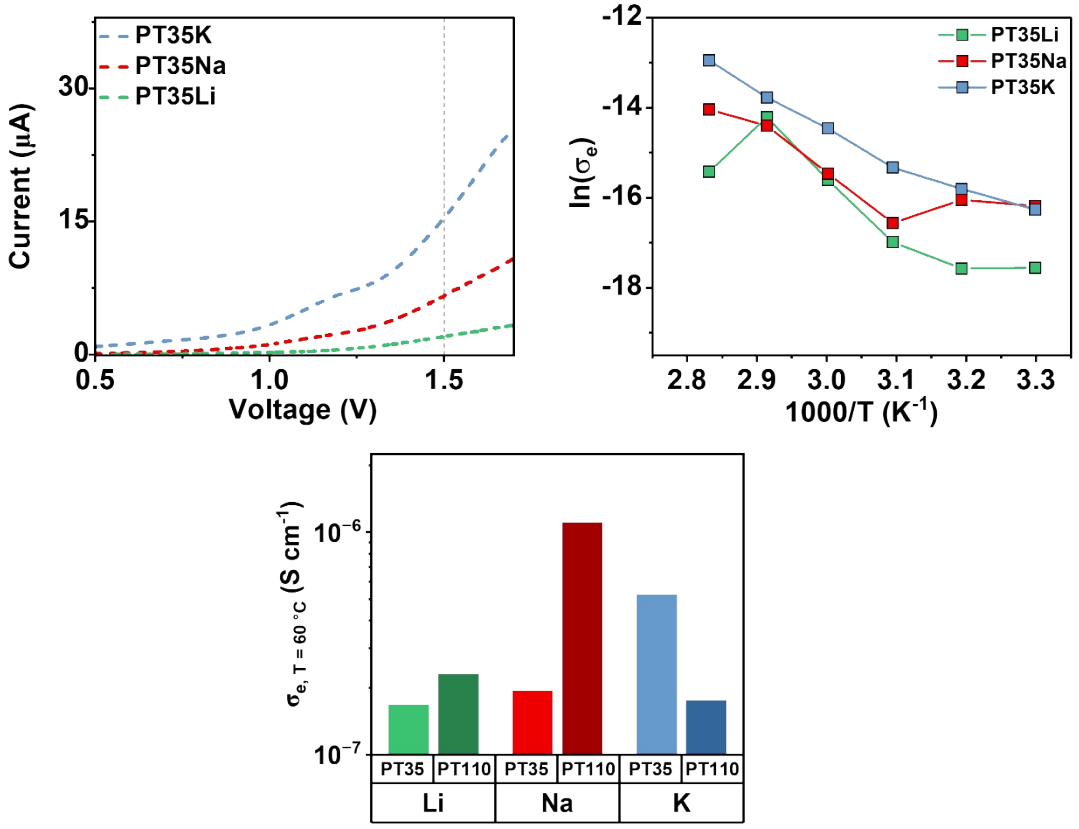

Fig. S16: LSV and temperature dependence of electronic conductivity (by CA) for PT35.

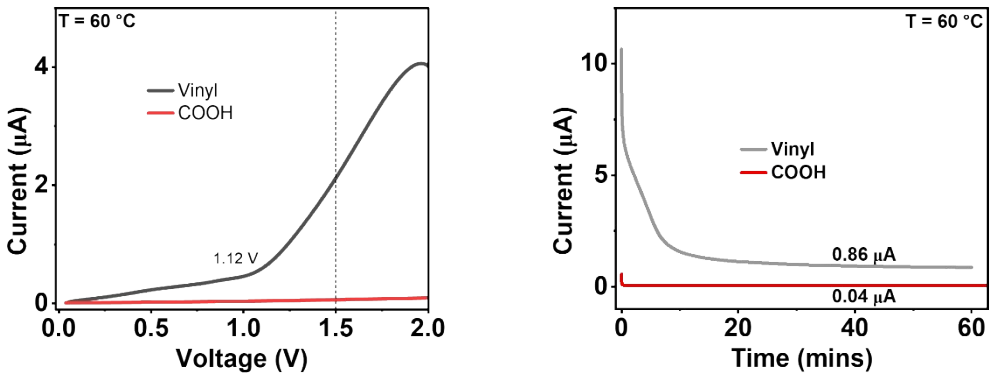

Fig. S17: CA and LSV for vinyl- and diacid-CBE controls.

P3HT wt%

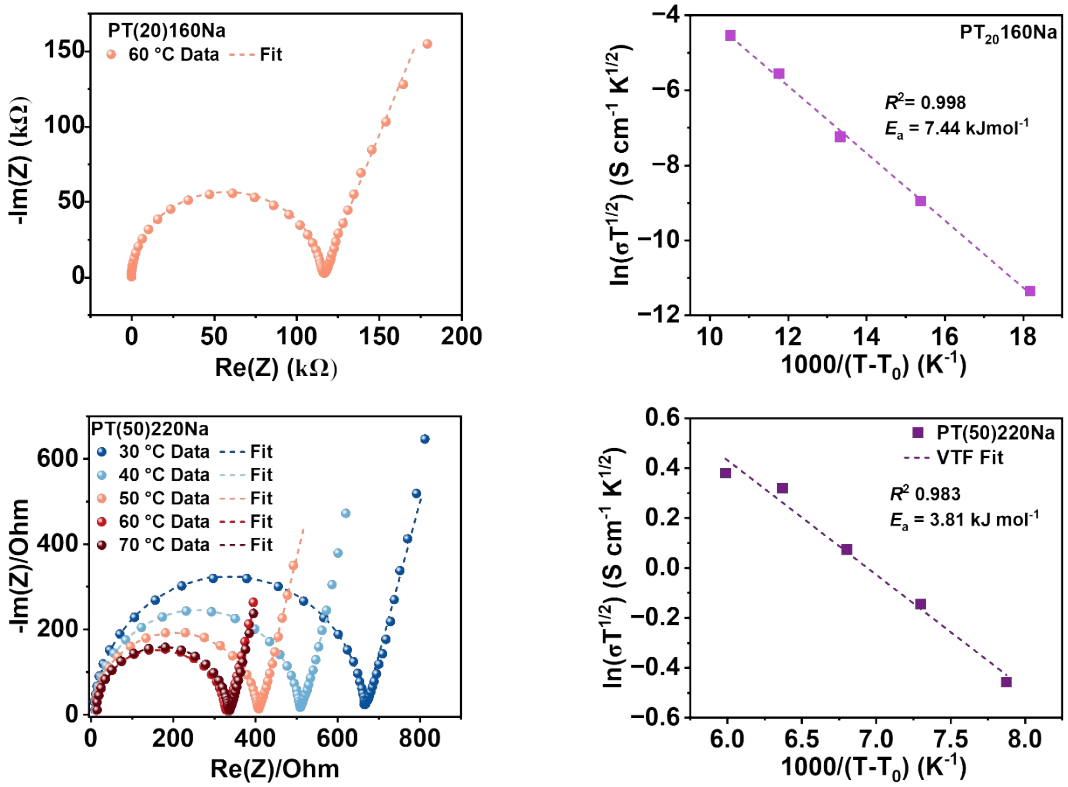

Fig. S18: Ionic conductivity measurements for 20 and 50 wt% P3HT CBEs.

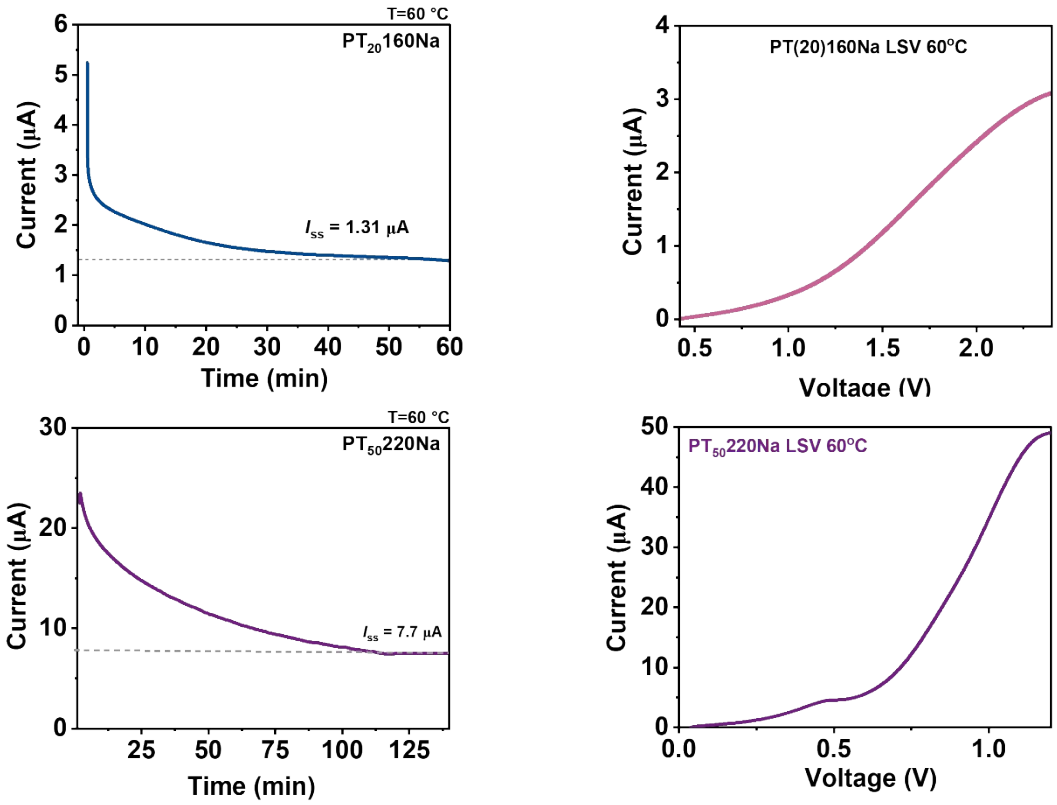

Fig. S19: Electronic conductivity measurements for 20 and 50 wt% P3HT CBEs.

Additional Tensile Testing and Mechanical Data

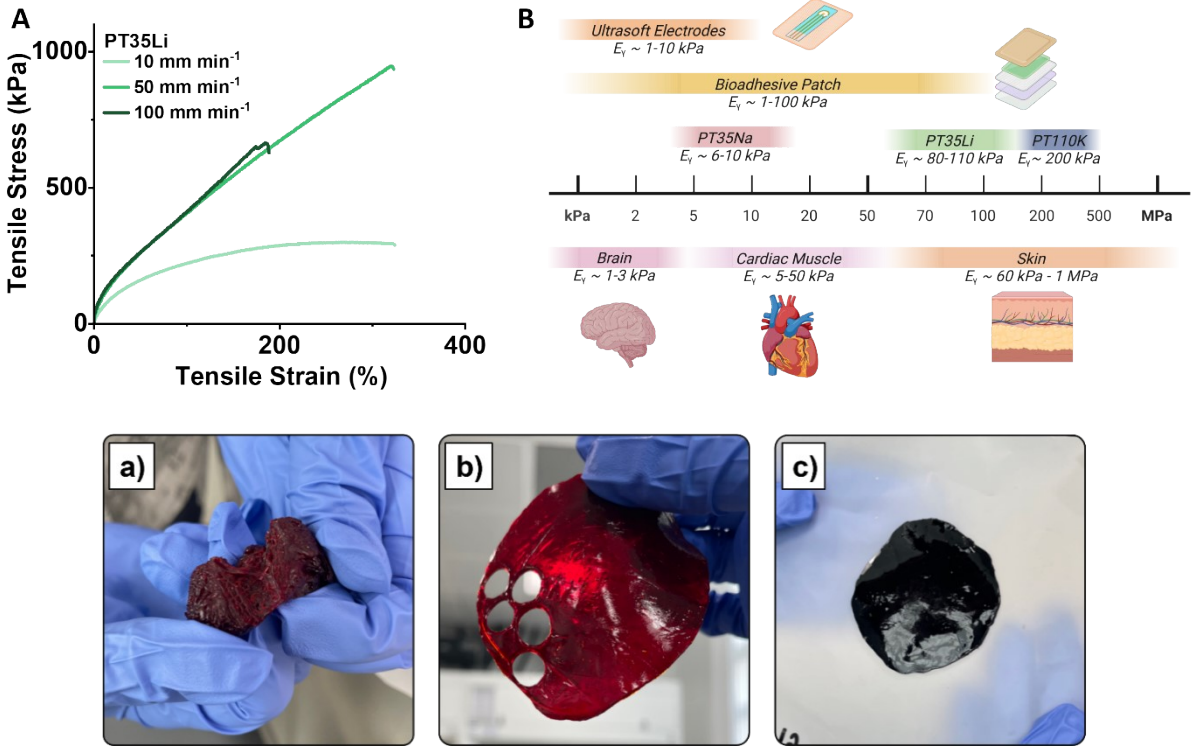

Fig. S20: (A) Additional stress-strain curves. (B) Comparison of CBEs in this work to the moduli of biological materials. (C) Photos of synthesised Na^+ based CBEs of varying DPs.

Density Functional Theory (DFT)

Calculations were performed using the Gaussian 16 suite of codes (revision C.01).[7] Input .gjf files were created and outputs visualised in GaussView 6.[8] Geometry optimisations were performed at 298 K using the ωB97XD hybrid functional with empirical dispersion correction developed by Chai and Head-Gordon,[9] which has been shown to perform well for conjugated polymers.[10, 11] A basis set of 6-311G(d,p) was used, with additional calculations performed using the diffuse 6-311+G(d,p) basis set to better describe the anionic borate. Solvent effects were modelled using the self-consistent reaction field (SCRF) approach with the conductor-like polarizable continuum model (CPCM) for DMSO. Frequency calculations confirmed all stationary points as minima by the absence of imaginary frequency modes. Multiple geometry optimisations were performed from different starting conformers to locate global minima; however, due to the size of these systems, we cannot exclude that some optimised geometries represent local rather than global minima. Computed energies are reported for a fixed side-chain stereochemistry for consistency. Output .chk files were converted to .fchk files for visualisation of molecular orbitals. Surfaces were visualised in GaussView at isovalue = 0.02 with coarse grain grid.

Table S2: Computed Energies: Ion Coordination Environment (Fig 6A).[a]

$\Delta G_{binding\ energy} = G_{Complex-CBE} - G_{M+} - G_{Anionic\ CBE}$

Where complex-CBE = $M^+BO_4^-$ (M-Borate), M^+-Borate-Ether; M^+-Ether and M^+-Ether-Thiophene complexes.

Structure[b]	***G* (Hartrees)**	**$\Delta G_{binding\ energy}$ (kcal mol^{-1})**
Li^+	-7.49757100	-
Na^+	-162.247714	-
K^+	-599.893245	-
Anionic CBE	-3547.821083	-
Li-Borate CBE	-3555.324580	**-3.72 (-0.80, -3.89)**[c, d]
Na-Borate CBE	-3710.075471	**-4.19 (-1.87, -4.04)**[c, d]
K-Borate CBE	-4147.722245	**-4.97 (-2.70, -3.99)**[c, d]
Li-Borate Ether CBE	-3555.350394	**-19.9**
Na-Borate Ether CBE	-3710.099380	**-19.2**
K-Borate Ether CBE	-4147.737759	**-14.7**

Li-Ether CBE	-3555.344418	**-16.2**
Na-Ether CBE	-3710.096616	**-17.5**
K-Ether CBE	-4147.739686	**-15.9**
Li-Ether Thiophene CBE	-3555.342588	**-15.0**
Na-Ether Thiophene CBE	-3710.091215	**-14.1**
K-Ether Thiophene CBE	-4147.735428	**-13.2**

[a] Level of theory: ωb97xd/6-311G(d,p)/cpcm=DMSO. [b] Model structures comprise one 3-hexylthiophene units (3HT), one polyether repeat unit with a pendant oligoether side chain (4 EO units) and one borate-functionalised polycarbonate repeat unit. [c] Diffuse basis set applied: 6-311+G(d,p). [d] Model structure extended to three 3HT units.

Table S3: Computed Energies: Polarons (Fig 6B). [a]

$\Delta\varepsilon_{DFT}^{HOMO-LUMO\ gap} = \varepsilon_{DFT}^{LUMO} - \varepsilon_{DFT}^{HOMO}$

Structure [b]	HOMO (eV)*	LUMO (eV)	HOMO-LUMO Gap (eV)
Anionic CBE (neutral P3HT)	-7.85	0.41	8.26
Polaron CBE (Linear)	-7.89	-1.40	6.49
Polaron CBE (Coiled)	-7.69	-1.08	6.61
BiPolaron CBE (Linear)	-9.47**	-4.01	5.26
BiPolaron CBE (Coiled)	-9.20	-3.74	5.45
Li-CBE (neutral P3HT)	-7.62	0.25	7.87
Na-CBE (neutral P3HT)	-7.62	0.24	7.86
K-CBE (neutral P3HT)	-7.62	0.24	7.86
Li-Polaron CBE (Linear)	-7.85	-1.35	6.50
Na-Polaron CBE (Linear)	-7.97	-1.41	6.55
K-Polaron CBE (Linear)	-7.97	-1.41	6.56
Li-BiPolaron CBE (Linear)	-9.43***	-3.97	5.46
Na-BiPolaron CBE (Linear)	-9.46***	-4.08	5.31
K-BiPolaron CBE (Linear)	-9.42***	-3.97	5.45

[a] Level of theory: ωb97xd/6-311G(d,p)/cpcm=DMSO. [b] Model structures comprise three 3-hexylthiophene units, one repeat unit with a pendant oligoether side chain (4 EO units), and one borate-functionalised polycarbonate repeat unit. *For bipolaron systems (doubly oxidised), the formal HOMO was localised on the electron-rich borate pendant group, so the highest occupied P3HT backbone-localised orbital was used for comparison with neutral and polaron systems: **HOMO-6, ***HOMO-2 (see Fig. S23).

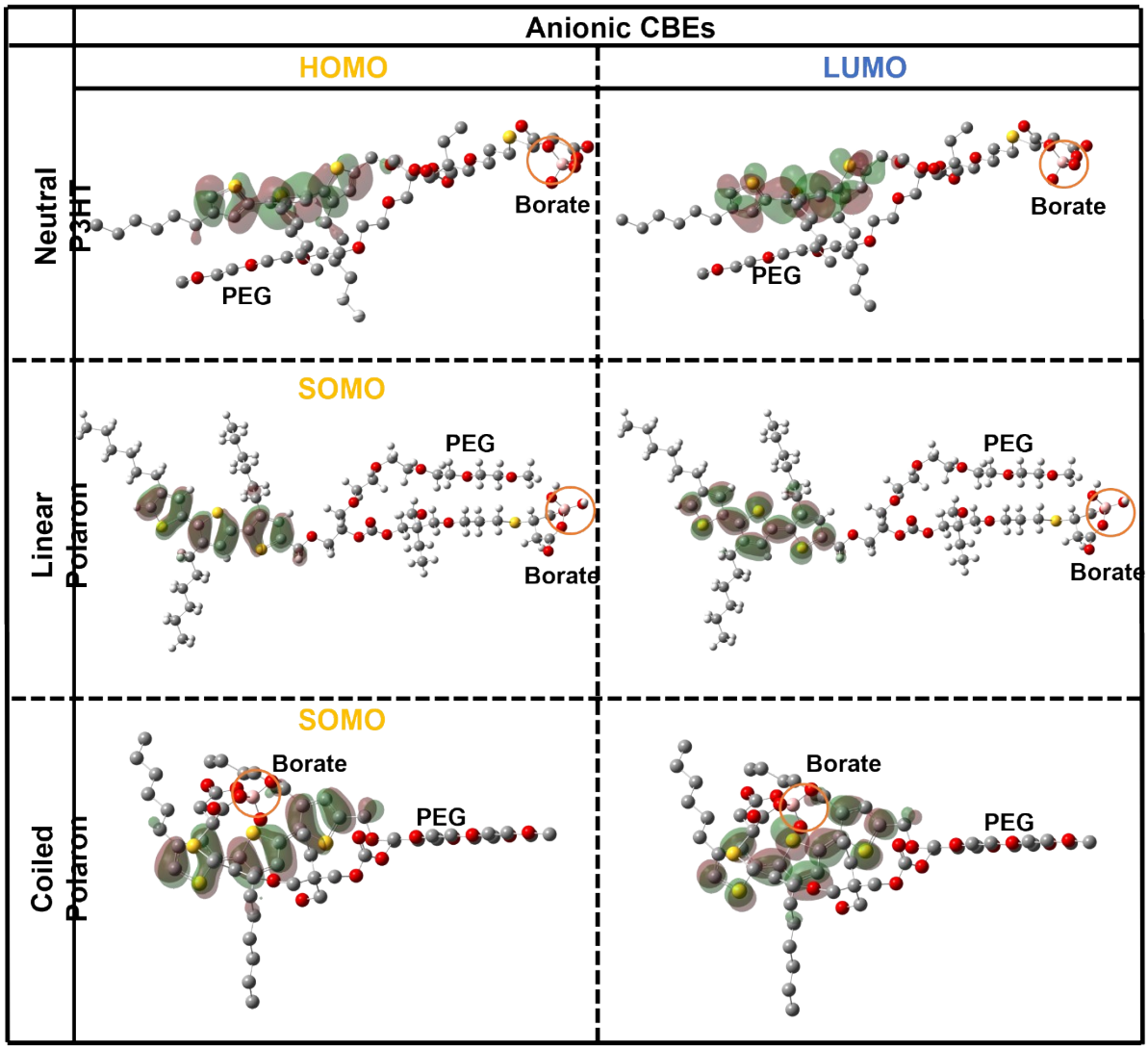

Fig. S21: HOMO-LUMO surfaces for Anionic CBEs; H atoms omitted for clarity.

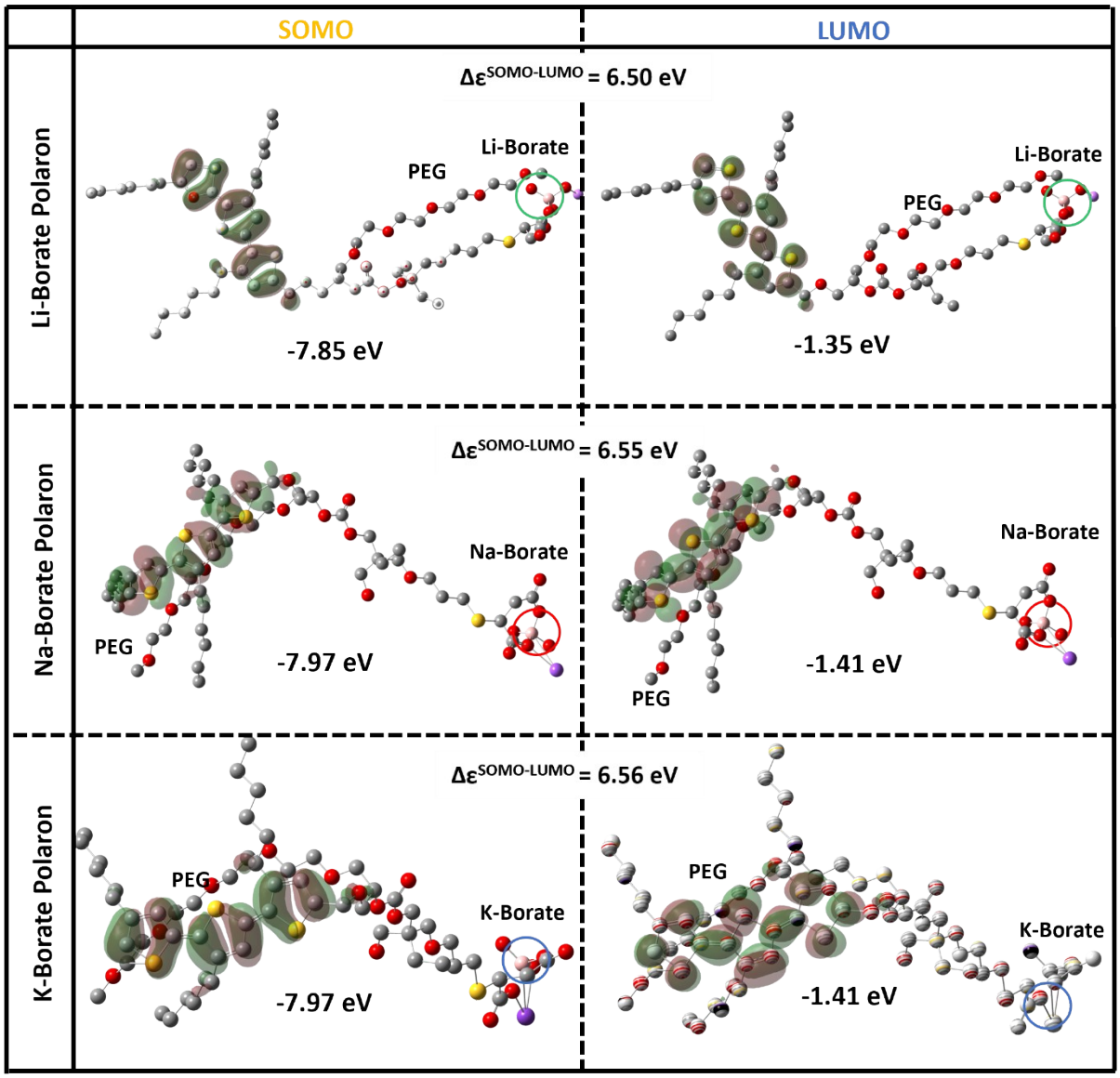

Fig. S22: HOMO-LUMO thiophene-based surfaces for Li, Na and K-CBEs; H atoms omitted for clarity.

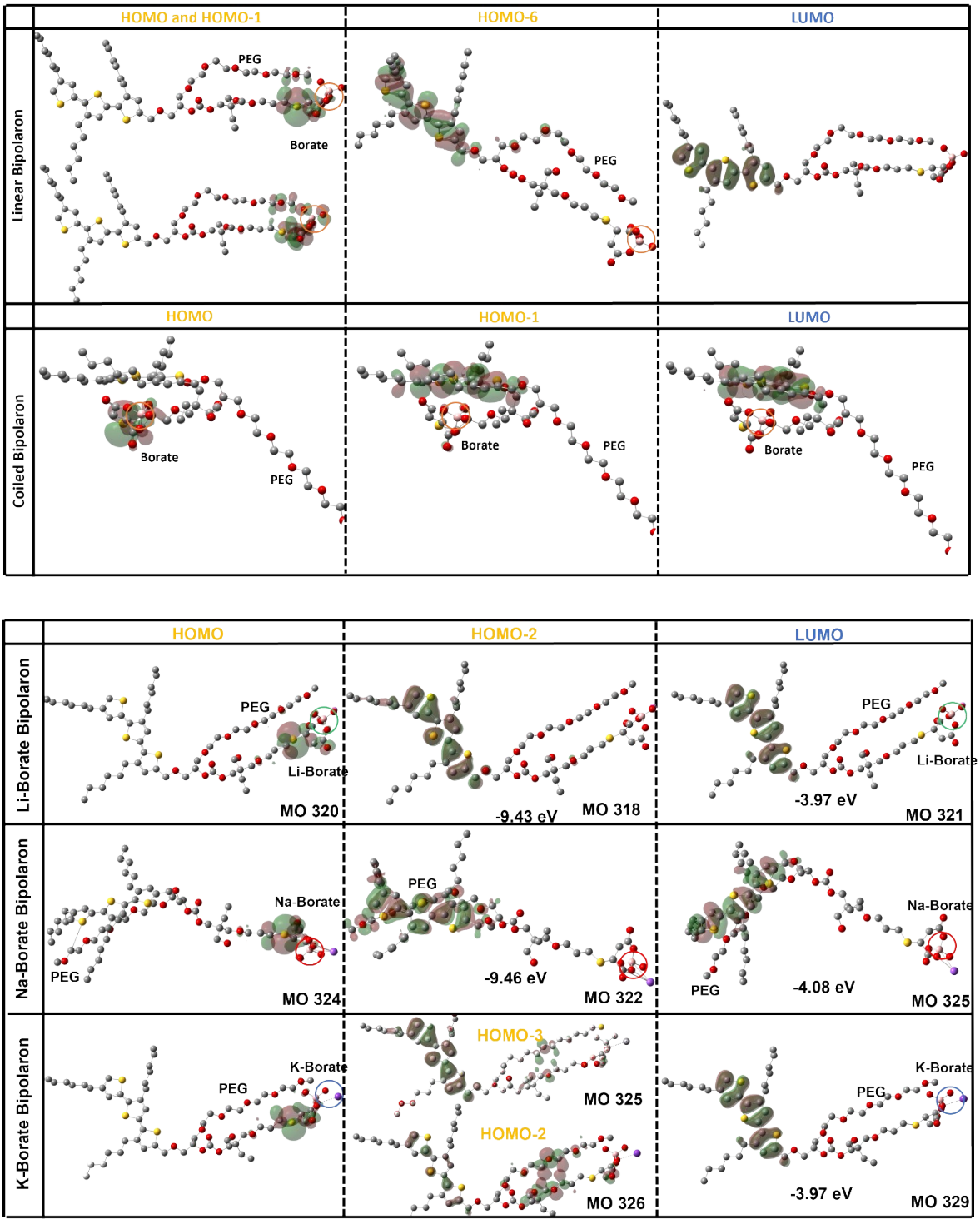

Fig. S23: HOMO-LUMO thiophene-based surfaces for bipolaron CBEs. Top: anionic CBE bipolarons; bottom: Li-, Na- and K-Borate bipolarons. Li: MO 319 = HOMO-1 Based on Borate (not shown); Na: MO 323 = HOMO-1 Based on Borate (not shown); H atoms omitted for clarity.

References

1. J. A. Carrillo, M. J. Ingleson and M. L. Turner, *Macromolecules*, 2015, **48**, 979–986.
2. V. Bagutski, A. Del Grosso, J. A. Carrillo, I. A. Cade, M. D. Helm, J. R. Lawson, P. J. Singleton, S. A. Solomon, T. Marcelli and M. J. Ingleson, *J. Am. Chem. Soc.*, 2013, **135**, 474–487.
3. J. Mindemark, L. Imholt, J. Montero and D. Brandell, *J. Polym. Sci. A: Polym. Chem.*, 2016, **54**, 2128–2135.
4. G. L. Gregory, G. S. Sulley, L. P. Carrodeguas, T. T. D. Chen, A. Santmarti, N. J. Terrill, K.-Y. Lee and C. K. Williams, *Chem. Sci.*, 2020, **11**, 6567–6581.
5. H.-N. Choi, H.-S. Yang, J.-H. Chae, T.-L. Choi and I.-H. Lee, *Macromolecules*, 2020, **53**, 5497–5503.
6. J. Lee, H. Park, S.-H. Hwang, I.-H. Lee and T.-L. Choi, *Macromolecules*, 2020, **53**, 3306–3314.
7. Gaussian 16 Rev. C.01, M. J. Frisch, G. W. Trucks, H. B. Schlegel, G. E. Scuseria, M. A. Robb, J. R. Cheeseman, G. Scalmani, V. Barone, G. A. Petersson, H. Nakatsuji, X. Li, M. Caricato, A. V. Marenich, J. Bloino, B. G. Janesko, R. Gomperts, B. Mennucci, H. P. Hratchian, J. V. Ortiz, A. F. Izmaylov, J. L. Sonnenberg, Williams, F. Ding, F. Lipparini, F. Egidi, J. Goings, B. Peng, A. Petrone, T. Henderson, D. Ranasinghe, V. G. Zakrzewski, J. Gao, N. Rega, G. Zheng, W. Liang, M. Hada, M. Ehara, K. Toyota, R. Fukuda, J. Hasegawa, M. Ishida, T. Nakajima, Y. Honda, O. Kitao, H. Nakai, T. Vreven, K. Throssell, J. A. Montgomery Jr., J. E. Peralta, F. Ogliaro, M. J. Bearpark, J. J. Heyd, E. N. Brothers, K. N. Kudin, V. N. Staroverov, T. A. Keith, R. Kobayashi, J. Normand, K. Raghavachari, A. P. Rendell, J. C. Burant, S. S. Iyengar, J. Tomasi, M. Cossi, J. M. Millam, M. Klene, C. Adamo, R. Cammi, J. W. Ochterski, R. L. Martin, K. Morokuma, O. Farkas, J. B. Foresman and D. J. Fox, Gaussian, Inc., Wallingford CT, 2016.
8. GaussView, Version 6, Roy Dennington, Todd A. Keith and John M. Millam, Semichem Inc. Shawnee Mission KS, 2016.
9. J.-D. Chai and M. Head-Gordon, *Phys. Chem. Chem. Phys.*, 2008, **10**, 6615–6620.
10. E. C. Wu and B. J. Schwartz, *J. Chem. Theory Comput.*, 2023, **19**, 6761–6769.
11. H. Sun and J. Autschbach, *J. Chem. Theory Comput.*, 2014, **10**, 1035–1047.